CORE
Metadata, citation and similar papers at core.ac.uk
Provided by Technische Universität Dresden: Qucosa

Dieses Dokument ist eine Zweitveröffentlichung (Verlagsversion) /

This is a self-archiving document (published version):

Stefan Lagotzky, Roman Barday, Andreas Jankowiak, Thorsten Kamps, Carola Klimm, Jens Knobloch, Günter Müller, Boris Senkovskiy, Frank Siewert

Prevention of electron field emission from molybdenum substrates for photocathodes by the native oxide layer

Erstveröffentlichung in / First published in:

The European physical journal : Applied Physics. 2015, 70(2), S. 21301-p1 – 21301-p8 [Zugriff am: 19.03.2020]. Cambridge University Press. ISSN 1286-0050.

DOI: https://doi.org/10.1051/epjap/2015150167

Diese Version ist verfügbar / This version is available on:

https://nbn-resolving.org/urn:nbn:de:bsz:14-qucosa2-390224

„Dieser Beitrag ist mit Zustimmung des Rechteinhabers aufgrund einer (DFGgeförderten) Allianz- bzw. Nationallizenz frei zugänglich."

This publication is openly accessible with the permission of the copyright owner. The permission is granted within a nationwide license, supported by the German Research Foundation (abbr. in German DFG).
www.nationallizenzen.de/

SLUB
Wir führen Wissen.

TECHNISCHE UNIVERSITÄT DRESDEN

QUCOSA
Quality Content of Saxony

Eur. Phys. J. Appl. Phys. (2015) 70: 21301
DOI: 10.1051/epjap/2015150167

THE EUROPEAN PHYSICAL JOURNAL APPLIED PHYSICS

Regular Article

Prevention of electron field emission from molybdenum substrates for photocathodes by the native oxide layer

Stefan Lagotzky[1,a], Roman Barday[2], Andreas Jankowiak[2], Thorsten Kamps[2], Carola Klimm[2], Jens Knobloch[2], Günter Müller[1], Boris Senkovskiy[3], and Frank Siewert[2]

[1] Bergische Universität Wuppertal, FB C Abteilung Physik, Gauss-Str. 20, 42097 Wuppertal, Germany
[2] Helmholtz-Zentrum Berlin für Materialien und Energie GmbH, Hahn-Meitner-Platz 1, 14109 Berlin, Germany
[3] Institut für Festkörperphysik, TU Dresden, 01069 Dresden, Germany

Received: 20 March 2015 / Accepted: 21 April 2015
Published online: 25 May 2015 – © EDP Sciences 2015

Abstract. Comprehensive investigations of the electron field emission (FE) properties of annealed single crystal and polycrystalline molybdenum plugs, which are used as substrates for actual alkali-based photocathodes were performed with a FE scanning microscope. Well-polished and dry-ice cleaned Mo samples with native oxide did not show parasitic FE up to a field level of 50 MV/m required for photoinjector cavities. In situ heat treatments (HT) above 400 °C, which are usual before photocathode deposition, activated field emission at lower field strength. Oxygen loading into the Mo surface, however, partially weakened these emitters. X-ray photoelectron spectroscopy of comparable Mo samples showed the dissolution of the native oxide during such heat treatments. These results reveal the suppression of field emission by native Mo oxides. Possible improvements for the photocathode preparation will be discussed.

1 Introduction

Molybdenum is often used in fundamental research and industry, e.g. as substrate for high quantum efficiency semiconductor photocathodes like Cs_2Te or CsK_2Sb [1–5]. These are utilized for the generation of high brightness electron beams in normal conducting as well as superconducting [6] radio-frequency (SRF) photoinjector cavities. Operation at high electric fields on the cathode surface is required to obtain a low electron beam emittance, thus increasing the probability of field emission (FE) from the cathode surface. Such photoinjectors, however, often suffer from dark currents due to parasitic FE, which limit the electric field on the photocathode surface to about 20 MV/m [7–9]. Usually, only the center of the Mo plug is coated with the photocathode material to reduce the production of an unwanted beam through stray laser light. Hence substrate material is also exposed to the RF field and parasitic FE can limit the performance of the injector cavity. Usually, the Mo substrate is heated in situ over 400 °C before the photocathode deposition to release absorbed gases and dissolve the native oxide layer [1,10], which might activate FE similarly as for Nb [11]. Therefore, FE from Mo must be investigated and prevented.

The interest in Mo is beyond the cathode preparation. For example, the compact linear collider (CLIC) is very demanding in terms of the peak surface field and requires a peak field of 243 MV/m with low FE and breakdown rate. It was proposed to use Cu accelerator cavities with refractory metal irises, and surface fields up to 420 MV/m were achieved in such 30 GHz structures [12]. Comparative dc spark measurements on Cu and Mo samples confirmed increased breakdown fields and decreased field enhancement factors [13–15]. Nevertheless, the origin of FE and its dependence on heat treatments (HT) remained unclear.

Mo is also used as a carrier for GaAs photocathodes, which are e.g., used for the generation of polarized electron beams in a 100 keV [16] or an unpolarized electron beam in a 500 keV [17,18] dc gun. Similar to our application, the GaAs-photocathode on a Mo plug is heated to about 550 °C to remove oxides and carbon contaminations from the photocathode surface prior to the final in situ activation of the GaAs surface to negative electron affinity and transfer into the gun cavity.

Systematic investigations of various electrode materials like molybdenum, titanium and stainless steel revealed that a combination of a molybdenum cathode and a titanium anode provides the best FE performance for high field dc electron guns [19]. Therefore, Mo electrodes are used for example in a 40 keV spin-polarized transmission electron microscope [20].

For all of these applications, a deep understanding of FE from the naturally oxidized or heated Mo surface is required. Therefore, we have systematically investigated

[a] e-mail: s.lagotzky@uni-wuppertal.de

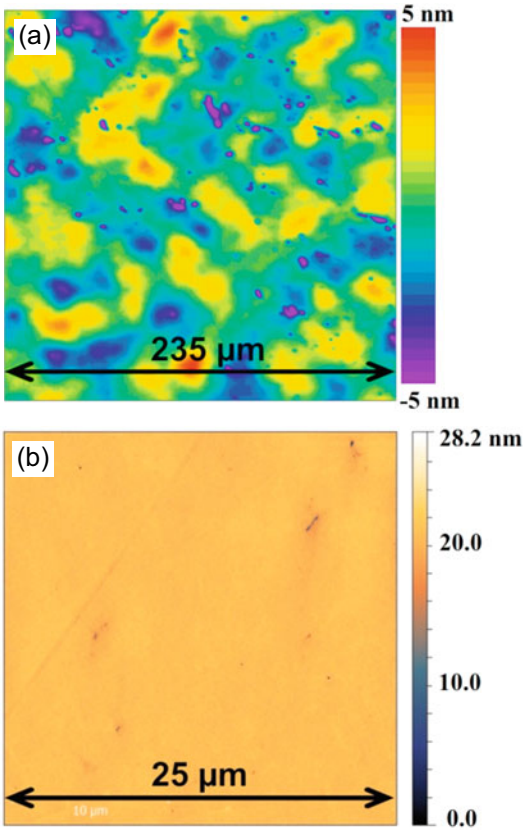

Fig. 1. Surface quality of the single crystal Mo sample measured by a white-light interferometer (a) and AFM (b). Measurements were performed prior to dry ice cleaning.

the FE from Mo before and after HT. Additionally, X-ray photoelectron spectroscopy (XPS) of similarly heated Mo surfaces was used to reveal the actual oxide structure.

2 Experimental details

2.1 Mo samples

Two Mo samples with a diameter of 10 mm and a rounded edge with $r \sim 0.3$ mm were investigated. Such Mo plugs are used as substrates for semiconductor photocathodes in SRF injector cavities [21,22]. A single crystal Mo sample was mechanically polished to a RMS surface roughness in the flat part of about $S_q < 2$ nm and peak-to-valley of $S_t < 40$ nm as measured by a white-light interferometer on a view field of 235 μm^2 and a $S_q < 1$ nm as measured by an atomic force microscope (AFM) in non-contact mode on a view field of 25 μm^2 (Fig. 1). A polycrystalline Mo sample was polished to a S_q of about 3 nm. Both samples were first cleaned with ionized nitrogen (SIMCO, PG-5) and then by dry-ice cleaning (DIC, CryoSnow, SJ-10) under ISO class 2 cleanroom conditions. It is remarkable that the single crystal sample received only one times DIC for 5 min, but the polycrystalline sample three times DIC for altogether 15 min. Finally, the samples were protected by a DIC Teflon® cap (2 min) to avoid any surface damage or dust contamination during transport.

2.2 Field emission scanning microscope (FESM)

The FE properties of the Mo samples were investigated in the FESM (see Fig. 2) at a vacuum pressure of about 10^{-7} Pa as described in detail elsewhere [23]. At first, each sample was tilt-corrected with respect to the truncated cone anode of 300 μm in diameter to achieve a constant gap Δz of at least 50 μm and correspondingly constant macroscopic electric field $E = V/\Delta z$ within ±10% over the flat part of the plug. Then all emitters which generate a FE threshold current I of 1 nA up to the given maximum voltage $V_{\max}$ were localized by means of PID-regulated scans $V(x, y)$ for a step width of $\Delta x = \Delta y = 150$ μm. Accordingly, emitter distribution maps with 67×67 points for a scan area of 1 cm^2 were obtained at a given $E_{\max}$ of 50 or 100 MV/m. All data were taken and recorded by a LabVIEW®-based software.

Guided by these maps local $V(z)$ and $I(E)$ measurements were carried out to calibrate the actual onset field E_{on} for 1 nA as well as to get the field enhancement factor β and the effective emitting area A_e of the emitter by a fit to the modified Fowler-Nordheim (FN) equation [24]:

$$I = A_e a \left(\beta E\right)^2 \varphi^{-1} t_N^{-2} \exp\left(-b\varphi^{1.5} \nu_N \left(\beta E\right)^{-1}\right). \quad (1)$$

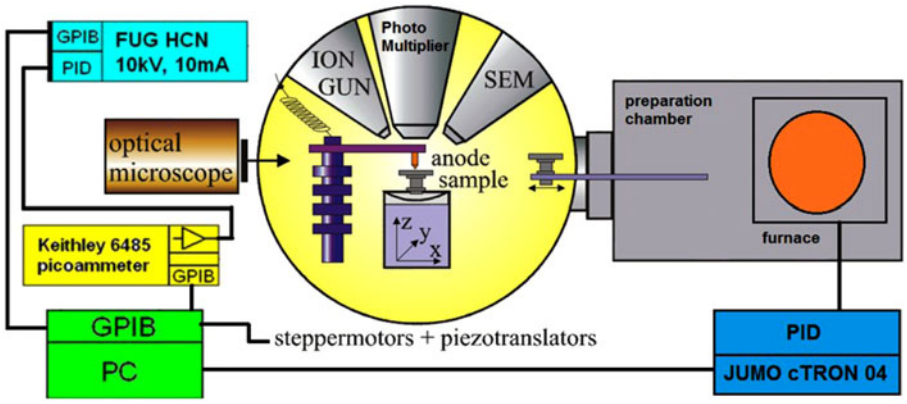

Fig. 2. Schematic view of the FESM.

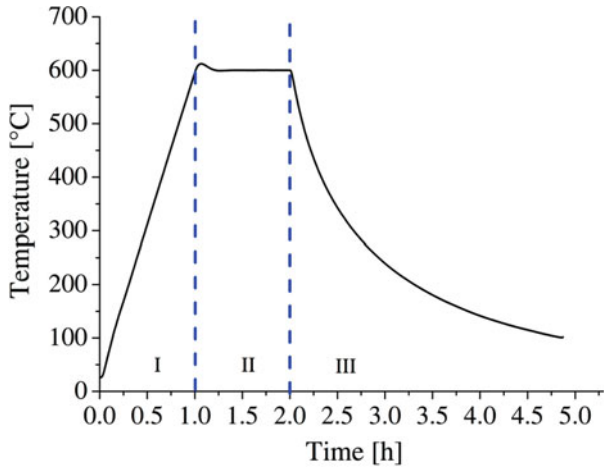

Fig. 3. Temperature profile during heat treatment (HT) up to 600 °C with linear ramp (I), annealing time (II) and natural cool down (III).

For I in A, A_e in m^2, φ in eV (was set to 4.3 eV for Mo), and E in V/m, $a = 1.54 \times 10^{-6}$ A eV V^{-2} and $b = 6.83 \times 10^9$ eV$^{-1.5}$ V m^{-1} are constants, t_N and ν_N are tabulated dimensionless functions of φ and E [25,26], which were set to 1 for simplicity. It should be noted, that equation (1) assumes a single emitter and is not valid for a large area surface with several emitting sites.

For the in situ HT of the Mo samples a resistively heated furnace in the preparation chamber of the FESM was used at about 10^{-5} Pa (see Fig. 2). Its temperature is measured with a thermocouple Pt10Rh-Pt and regulated with a PID controller (JUMO cTron 04). A typical temperature profile of a HT is given in Figure 3.

Most of the emitters were finally investigated by means of ex situ high resolution scanning electron microscopy (SEM) and energy-dispersive X-ray spectroscopy (EDX). By means of marks on the sample holder, the relocalization of an emitter region is possible within a precision of about 500 μm.

2.3 X-ray photoelectron spectroscopy (XPS)

The oxide structure of a comparable polycrystalline Mo sample of 99.9% purity was investigated by means of XPS at the Russian-German beamline of the synchrotron radiation source BESSY II [27]. The XPS spectra were taken at an incident photon energy of 650 eV and at a base vacuum pressure of about 4×10^{-8} Pa. A high resolution hemispherical energy analyzer PHOIBOS 150 (SPECS) was used to reveal the XPS spectrum of the Mo 3d level, which is very sensitive to oxide contaminations.

3 Results and discussion

3.1 FESM maps

In order to investigate the role of the natural oxide on the FE properties of Mo, six FE scans were performed on the whole area of the single crystal sample up to 50 MV/m which is a reasonable peak surface field for SRF cavity operation, i.e., as received and after HT at 200, 300, 400, 500 and 600 °C for about 1 h. No FE was observed after HT up to 400 °C, but 19 (26) emitters occurred after HT at 500 (600) °C as shown in Figures 4a and 4b. It is remarkable that a major part of these emitters are

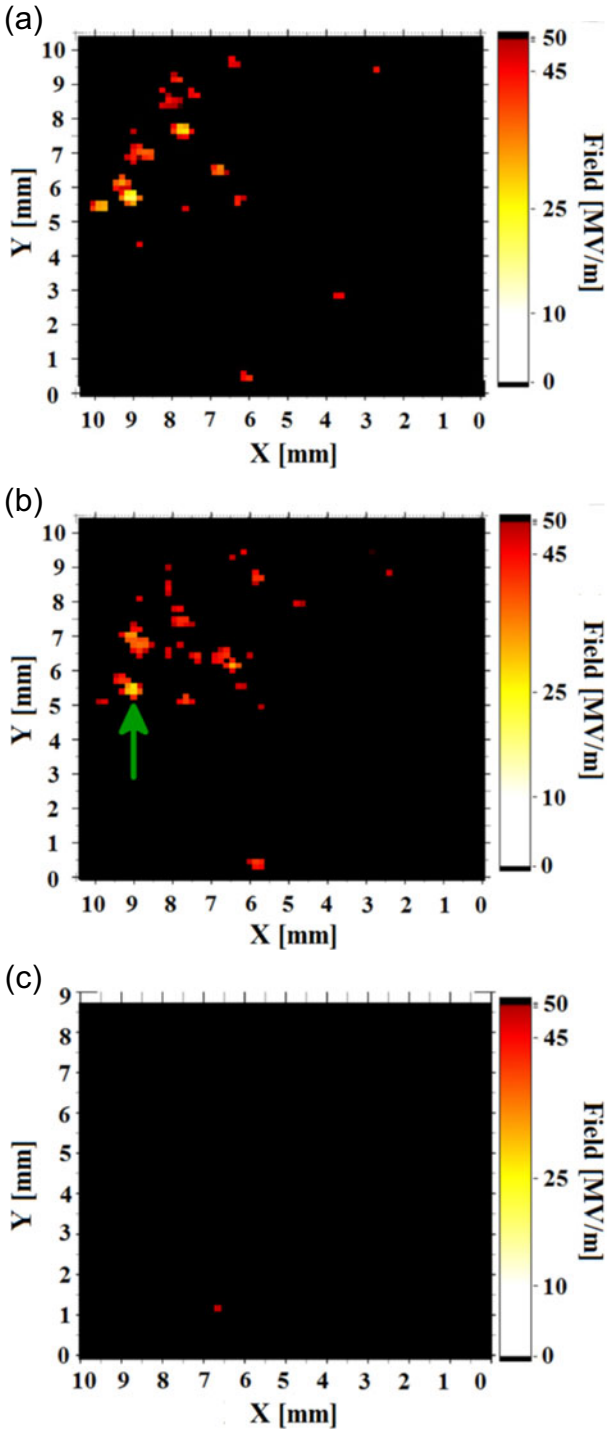

Fig. 4. FE maps up to $E = 50$ MV/m of the single crystal Mo sample after HT at 500 °C (a) and 600 °C (b) and of the much better cleaned polycrystalline sample after HT at 600 °C (c).

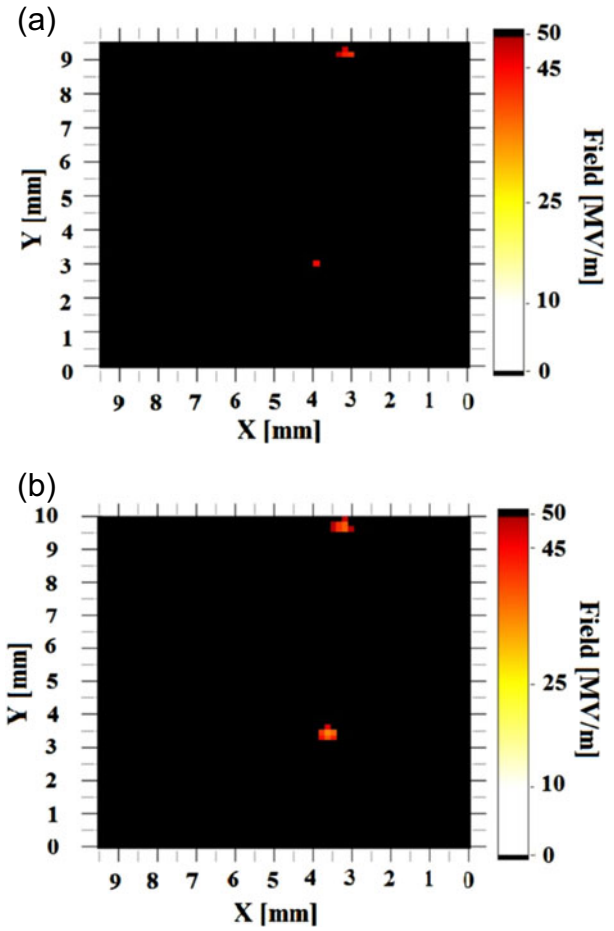

Fig. 5. FE maps of the polycrystalline Mo sample up to $E = 50$ MV/m after prompt venting of the vacuum chamber with O_2 (a) and after additional HT at 600 °C (b).

located near the edge of the sample, thus indicating a worse surface quality of the rounded edge. There are three strong emitters after the HT at 500 °C with $E_{on} \sim 20$ MV/m, which is relevant for the applications in RF cavities.

A comparable polycrystalline Mo sample was also stepwise investigated which, however, received a more careful preparation by longer DIC. Accordingly, no emitter was found in the FE maps up to 50 MV/m of the unannealed sample as well as up to HT at 500 °C, and a weak emitter ($E_{on} = 49$ MV/m) occurred after HT at 60 °C (Fig. 4c) but disappeared during the following local measurements. In order to get more emitters for the systematic study of the effect of oxide on FE, this Mo sample was exposed to 1 atm of oxygen gas from a bottle by prompt venting of the preparation chamber of the FESM without any effort for dust prevention. As expected, some μm-size particulates were observed on the Mo surface by means of the long-range optical microscope with CCD-camera (see Fig. 2). Nevertheless, the resulting FE maps in Figure 5a showed only two emitters up to 50 MV/m which became significantly stronger after HT at 600 °C (Fig. 5b).

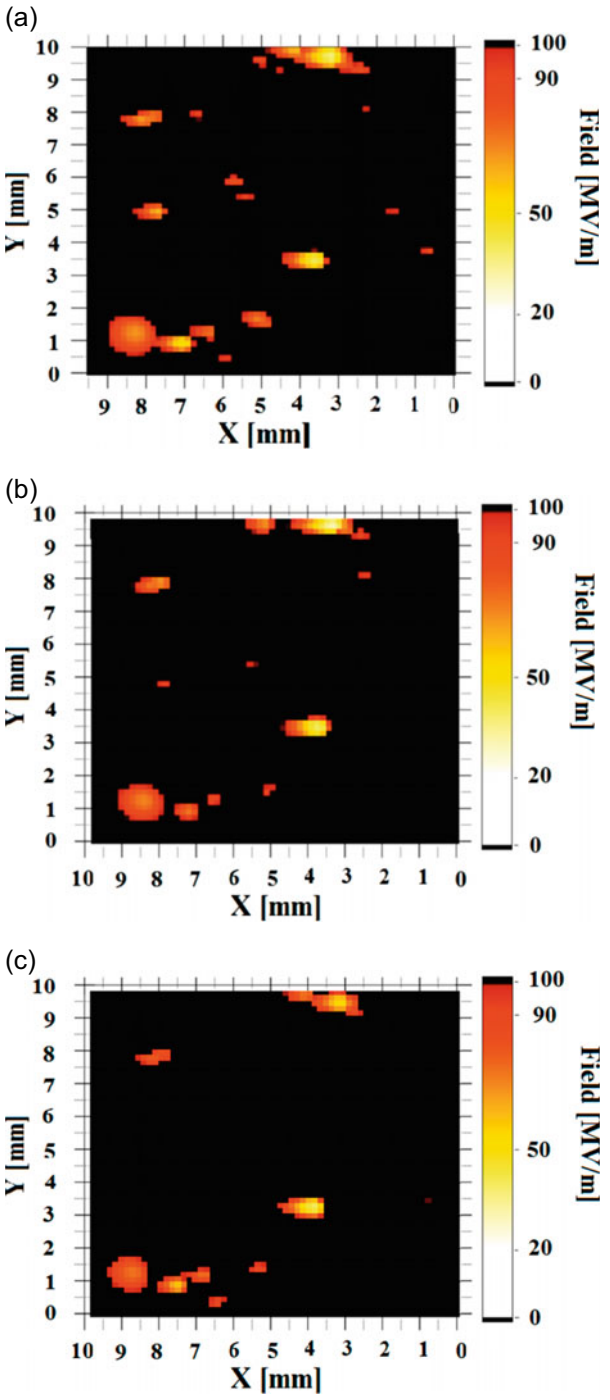

Fig. 6. FE maps of the polycrystalline Mo sample up to $E = 100$ MV/m after HT at 600 °C (a) and after different reoxidation steps with O_2 pressure: $p = 10^5$ Pa at 25 °C (b) and $p = 1$ Pa at 400 °C (c).

Finally, this polycrystalline Mo sample was scanned up to 100 MV/m to enhance its FE significantly. Beside both formerly present emitters, about 18 additional ones with E_{on} values of 30–90 MV/m could be activated now as shown in Figure 6a. It is remarkable that some new emitter show rather low values for E_{on} now. This well-known

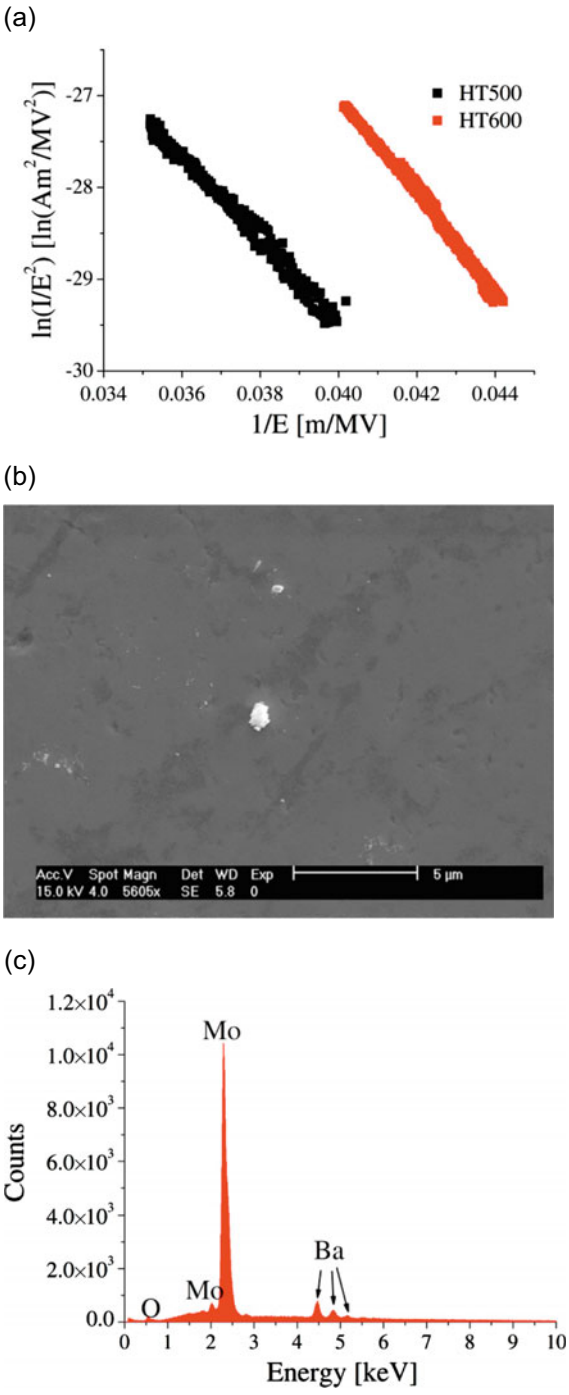

Fig. 7. Fowler-Nordheim plot of the activated emitter marked in Figure 4b (a) after HT at 500 °C (E_{on} = 29.5 MV/m, β = 133, $A_e = 2.1\times10^{-3}$ μm^2) and 600 °C (E_{on} = 25.3 MV/m, β = 114, $A_e = 8.65\times10^{-1}$ μm^2). The SEM image (b) and EDX spectrum (c) around the emission region revealed Ba particulates.

activation effect for field emitters is usually explained by the creation of conducting channels in the insulating oxide layer [11,28].

Therefore, this sample was well-suited to look for the reverse oxide effect, i.e., a suppression of FE by a thicker

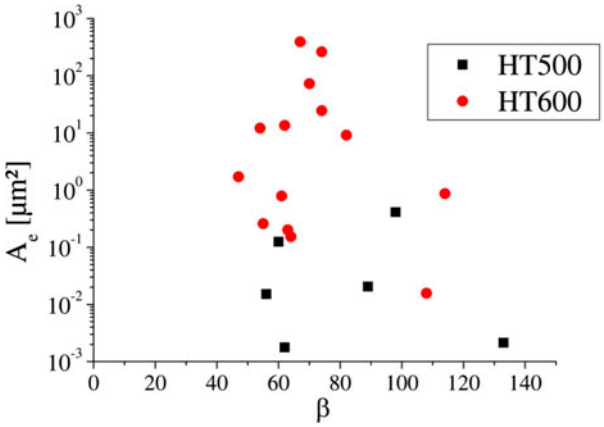

Fig. 8. Least square fit parameters A_e versus β of measured FN-plots for the strongest emitters in Figure 4 for a work function φ = 4.3 eV.

oxide which was realized in the preparation chamber of the FESM by two steps: at first a slow venting over 1 h to 1 atm with filtered oxygen and then by a HT at 400 °C and 1 Pa for 0.5 h. As expected, some weak emitters disappeared in the maps (Figs. 6b and 6c), and most of the others were significantly weakened.

Based on these FESM maps of both samples, there is already a statistical evidence for the enhancement of FE by dissolution of the insulating oxide as well as the suppression of FE by the native or in situ grown Mo oxide. More challenging, however, remains a study of the according change of the FE from individual emitters.

3.2 Characterization of single emitters

The *I-V* curves of most of the emitters found on the single crystal Mo sample (see Figs. 4a and 4b) were measured after HT at 500 and 600 °C. Moreover, SEM images and EDX spectra were ex situ taken in the emitter regions. In Figure 7, a typical example for the strengthening of a field emitter by HT at the higher temperature is given which is most probably a particulate with Ba content. Beside the 15% reduced E_{on} value, the resulting FN parameters of this emitter hint for an increased size of A_e rather than for a higher β value.

Similar results were obtained for most emitters on this sample, i.e., nearly stable FN-like *I-V* curves with slightly changed fit parameters which are summarized in Figure 8. Obviously, their effective emitting area A_e becomes larger on average, while the range of β values remains unchanged. It is remarkable that a few emitters yielded much higher unreasonable $A_e > 10^4$ μm^2 which hint for resonant tunneling effects [29] due to adsorbates [30] or thin oxide layers [31]. Moreover, careful SEM studies revealed only particulates as origin of the parasitic FE, and no surface defects were found on the well-polished Mo surface.

Local measurements of the strongest emitters were also performed on the polycrystalline Mo sample after

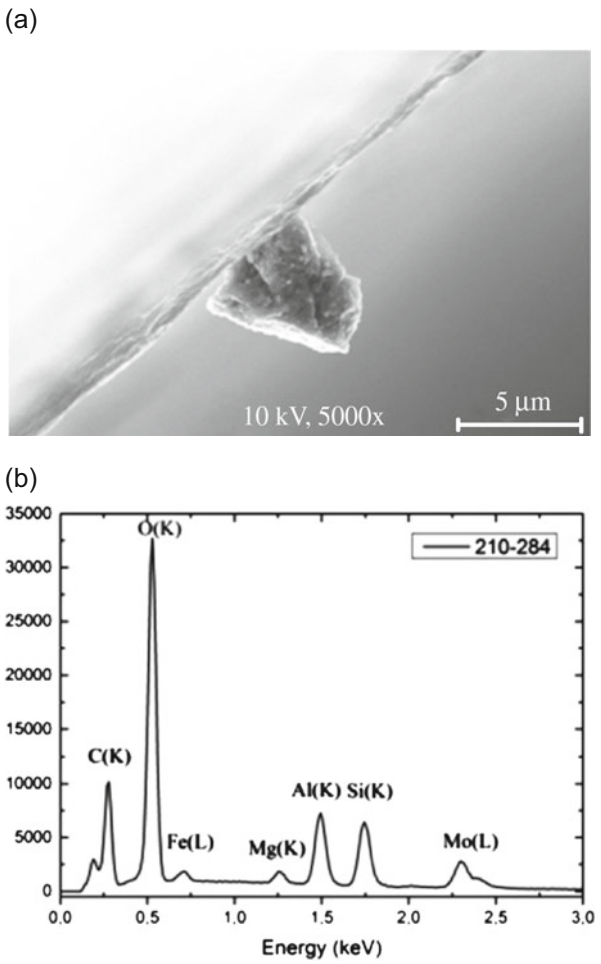

Fig. 9. SEM image (a) and EDX spectrum (b) of a non-emitting particulate, which occurred on the surface after prompt venting with O_2.

all the three steps shown in Figure 6. Similar results in terms of stable *I-V* curves and FN fit parameters were obtained. Due to the prompt venting, however, much more particulates than emitters were found in the SEM images, most of which did not emit (e.g., Fig. 9). Therefore, further correlation studies between FE properties and morphology of these emitters were not possible for this sample.

3.3 X-ray photoelectron spectra

It is commonly known that formation of the oxides on the surface can significantly affect FE properties and particularly suppress FE [11,32]. To investigate the influence of HT on molybdenum oxides we used XPS, which is very sensitive to the chemical state of the surface. The shape of Mo $3d$ spectrum prior to HT reveals besides metallic molybdenum the presence of conducting MoO_2, semiconducting MoO_3 (energy gap of 3 eV and a work function of 6.9 eV [33]) and nonstoichometric MoO_x

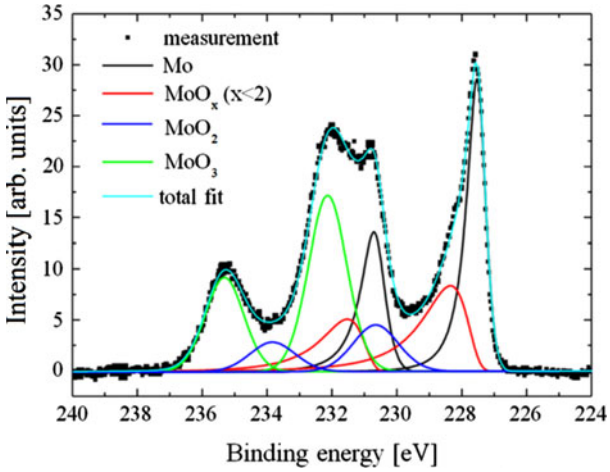

Fig. 10. Mo $3d$ photoemission spectrum prior to HT with deconvolution and corresponding fit curves.

Table 1. Estimated weights of individual oxides and thickness of the total Mo oxide layer.

Treatment	f (MoO_2)	f (MoO_3)	h (nm)
As received	0.11	0.33	3.5
100 °C	0.14	0.11	2.7
300 °C	0.14	0.05	1.9
400 °C	0.00	0.00	1.1

oxides (Fig. 10). After deconvolution of the spectrum the weight of each component f is obtained as a ratio of the area under the corresponding peak to the total area of the spectrum.

After the XPS measurement the sample was moved into a preparation chamber for a HT. Four treatment cycles were performed in situ with increasing temperature of 100, 300, 400 and 600 °C for 1 h. After each treatment step the sample was transferred back into the analyzing chamber for the XPS measurement. The position of the illuminated area remains unchanged. The weight f for MoO_3 reduces from ∼0.33 for the unannealed sample to 0.05 after HT at 300–600 °C (see Tab. 1). After HT at 400 °C the molybdenum trioxide layer is dissolved into the bulk (Fig. 11). After the last HT at 600 °C all Mo oxide correlated peaks disappeared, indicating that the oxide film was removed completely. The thickness of the oxide layer can be estimated as:

$$h = -\lambda \times \ln(I/I_0), \tag{2}$$

where λ is the electron inelastic mean free path (IMFP) in the oxide layer, I and I_0 are the intensities of metallic component in the XPS spectra with and without oxide layer, respectively. For MoO_3 and an electron energy of 420 eV, $\lambda \sim 1.1$ nm and for other oxides IMFP is nearly the same [34]. Therefore, the total oxide layer thickness prior to HT can be estimated as $h \sim 3.5$ nm (Tab. 1).

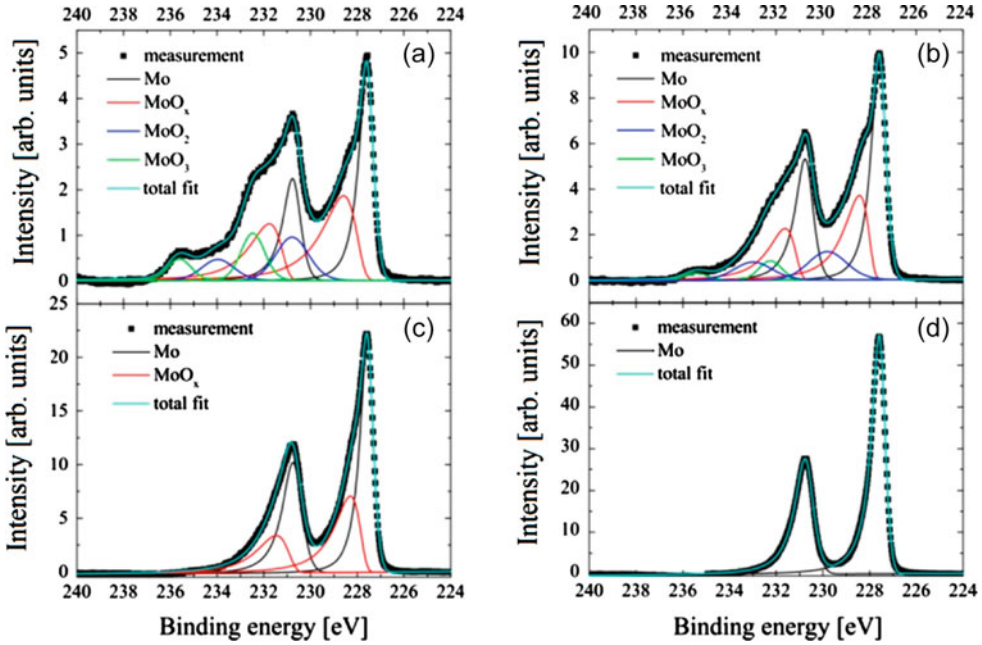

Fig. 11. Mo 3*d* photoemission spectra after HT at 100 °C (a), 300 °C (b), 400 °C (c) and 600 °C (d).

4 Conclusion

Insulating oxides naturally present on well-polished single crystalline as well as polycrystalline Mo samples prevent parasitic FE up to 50 MV/m. HT for about 1 h above 400–500 °C, however, activate FE with E_{on} values as low as 20 MV/m especially from rough particulates which are still present despite of DIC. Exposure of the Mo surface to one atmosphere of pure oxygen or vacuum annealing under partial oxygen pressure partially weakened such emitters. Systematic XPS spectra after comparable HT revealed the dissolution of MoO_3 due to oxygen diffusion into the bulk, thus explaining the enhanced FE of in situ annealed samples. The preparation of semiconductor photocathodes, however, requires an oxide-free Mo surface. Selective removal of the oxide layer by a laser with a short pulse length solely in the photocathode region prior to the alkali-based material deposition might be the right solution to prevent FE from the surrounding naturally or artificially oxidized Mo substrates. Further investigations of FE in the presence of such layers and its influence on RF properties are required to improve the brilliance of the electron sources.

This work is supported in parts by the German Federal Ministry of Education and Research under Project number 05K13PX2, Land Berlin and grants of Helmholtz Association.

References

1. D. Sertore, P. Michelato, L. Monaco, S. Schreiber, J. Han, A. Bonucci, *Proc. of the 2005 Particle Accelerator Conf., Knoxville, Tennesse, 2005*, edited by C. Horak (IEEE, New York, 2005), p. 671, `http://www.jacow.org`
2. S.H. Kong, J. Kinross-Wright, D.C. Nguyen, R.L. Sheffield, J. Appl. Phys. **77**, 6031 (1995)
3. Z. Yusof, E. Wisniewski, L. Spentzouris, *Proc. of the 3rd Int. Particle Accelerator Conf., New Orleans, Louisiana, 2012*, edited by F. Zimmermann, C. Eyberger (IEEE, New York, 2012), p. 1569, `http://www.jacow.org`
4. E. Wang, T. Rao, I. Ben-Zvi, Phys. Rev. ST Accel. Beams **17**, 023402 (2014)
5. A. di Bona, F. Sabary, S. Valeri, P. Michelato, D. Sertore, G. Suberlucq, J. Appl. Phys. **80**, 3024 (1996)
6. J. Teichert et al., *Proc. of the 27th Int. Free Electron Laser Conf., Palo Alto, California, 2005*, edited by H.D. Nuhn (JACoW, Geneva, 2005), p. 534, `http://www.jacow.org`
7. R. Xiang, A. Arnold, T. Kamps, P. Lu, P. Michel, P. Murcek, H. Vennekate, G. Staats, J. Teichert, Phys. Rev. ST Accel. Beams **17**, 043401 (2014)
8. R. Huang, D. Filippetto, C.F. Papadopoulos, H. Qian, F. Sannibale, M. Zolotorev, Phys. Rev. ST Accel. Beams **18**, 013401 (2015)
9. R. Barday, S. Lagotzky, A. Jankowiak, T. Kamps, C. Klimm, J. Knobloch, F. Siewert, A. Varykhalov, G. Müller, B. Senkovskiy, in *Proc. of the 5th Int. Particle Accelerator Conf., Dresden, 2014*, edited by Ch. Petit-Jean-Genaz (JACoW, Geneva, 2014), p. 2955, `http://www.jacow.org`
10. A. di Bona, F. Sabary, S. Joly, P. Mochelato, D. Sertore, C. Pagani, S. Valeri, Nucl. Instrum. Methods Phys. Res. A **385**, 385 (1997)
11. A. Navitski, S. Lagotzky, D. Reschke, X. Singer, G. Müller, Phys. Rev. ST Accel. Beams **16**, 112001 (2013)
12. W. Wuensch, C. Achard, S. Döbert, H.H. Braun, I. Syratchev, M. Taborelli, I. Wilson, *Proc. of the 2003 Particle Accelerator Conf., Portland, Oregon, 2003*, edited by J. Chew, P. Lucas, S. Webber (IEEE, New York, 2003), p. 495, `http://www.jacow.org`

13. M. Kildemo, S. Calatroni, M. Taborelli, Phys. Rev. ST Accel. Beams **7**, 092003 (2004)
14. A. Descoeudres, Y. Levinsen, S. Calatroni, M. Taborelli, W. Wuensch, Phys. Rev. ST Accel. Beams **12**, 092001 (2009)
15. H. Timko, M. Aicheler, P. Alknes, S. Calatroni, A. Oltedal, A. Toerklep, M. Taborelli, W. Wuensch, Phys. Rev. ST Accel. Beams **14**, 101003 (2011)
16. K. Aulenbacher, Ch. Nachtigall, H.G. Andresen, J. Bermuth, Th. Dombo, P. Drescher, H. Euteneuer, H. Fischer, D.V. Harrach, P. Hartmann, J. Hoffmann, P. Jennewein, K.H. Kaiser, S. Köbis, H.J. Kreidel, J. Langbein, M. Petri, S. Plützer, E. Reichert, M. Schemies, H.-J. Schöpe, K.-H. Steffens, M. Steigerwald, H. Trautner, Th. Weis, Nucl. Instrum. Methods Phys. Res. A **391**, 498 (1997)
17. R. Nagai, R. Hajima, N. Nishimori, T. Muto, M. Yamamoto, Y. Honda, T. Miyajima, H. Iijima, M. Kuriki, M. Kuwahara, S. Okumi, T. Nakanishi, Rev. Sci. Instrum. **81**, 033304 (2010)
18. N. Nishimori, R. Nagai, M. Yamamoto, Y. Honda, T. Miyajima, H. Iijima, M. Kuriki, M. Kuwahara, S. Okumi, T. Nakanishi, R. Hajima, J. Phys.: Conf. Ser. **298**, 012005 (2011)
19. F. Furuta, T. Nakanishi, S. Okumi, T. Gotou, M. Yamamoto, M. Miyamoto, M. Kuwahara, N. Yamamoto, K. Naniwa, K. Yasui, H. Matsumoto, M. Yoshioka, K. Togawa, Nucl. Instrum. Methods Phys. Res. A **538**, 33 (2005)
20. M. Kuwahara, Y. Takeda, K. Saitoh, T. Ujihara, H. Asano, T. Nakanishim, N. Tanaka, J. Phys.: Conf. Ser. **298**, 012016 (2011)
21. R. Xiang, A. Arnold, H. Buettig, D. Janssen, M. Justus, U. Lehnert, P. Michel, P. Murcek, A. Schamlott, Ch. Schneider, R. Schurig, F. Staufenbiel, J. Teichert, Phys. Rev. ST Accel. Beams **13**, 043501 (2010)
22. M. Abo-Bakr, W. Anders, R. Barday, A. Bondarenko, K. Bürkmann-Gehrlein, V. Dürr, S. Heßler, A. Jankowiak, T. Kamps, J. Knobloch, O. Kugeler, B. Kuske, P. Kuske, A. Matveenko, A. Meseck, G. Meyer, R. Müller, A. Neumann, K. Ott, Y. Petenev, D. Pflückhahn, T. Quast, J. Rahn, S. Schubert, *Conceptual Design Report BERLinPro*, edited by B. Kuske, N. Paulick, A. Jankowiak, J. Knobloch (Helmholtz-Zentrum Berlin, 2012), pp. 69–70
23. D. Lysenkov, G. Müller, Int. J. Nanotechnol. **2**, 239 (2005)
24. R.G. Forbes, J. Vac. Sci. Technol. B **17**, 534 (1999)
25. R.E. Burgess, H. Kroemer, J.M. Houston, Phys. Rev. **90**, 515 (1953)
26. H.C. Miller, J. Franklin Inst. **282**, 382 (1966)
27. S.I. Fedoseenko, D.V. Vyalikh, I.E. Iossifov, R. Follath, S.A. Gorovikov, R. Puttner, J.S. Schmidt, S.L. Molodtsov, V.K. Adamchuk, W. Gudat, G. Kaindl, Nucl. Instrum. Methods Phys. Res. A **505**, 718 (2003)
28. S. Lagotzky, G. Müller, in *Proc. of the 5th Int. Particle Accelerator Conf., Dresden, 2014*, edited by Ch. Petit-Jean-Genaz (JACoW, Geneva, 2014), p. 2258, `http://www.jacow.org`
29. C.B. Duke, M.E. Alferieff, J. Chem. Phys. **46**, 923 (1967)
30. T. Habermann, A. Göhl, D. Nau, G. Müller, H. Piel, M. Wedel, *Proc. of the 1997 Workshop on RF Superconductivity, Abano Terme, Italy, 1997*, edited by V. Palmieri (JACoW, Geneva, 1998), p. 972, `http://www.jacow.org`
31. J. Halbritter, Surf. Sci. **122**, 80 (1982)
32. R.V. Latham, *High Voltage Vacuum Insulation: Basic Concepts and Technological Practice*, edited by R.V. Latham (Academic Press, London, 1995)
33. M. Kröger, S. Hamwi, J. Meyer, T. Riedl, W. Kowalsky, A. Kahn, Appl. Phys. Lett. **95**, 123301 (2009)
34. `https://www.nist.gov/srd/nist71.cfms`